

# Solidified Fillings of Nanopores

Patrick Huber\* and Klaus Knorr  
*Technische Physik, Universität des Saarlandes, 66041 Saarbrücken, Germany*  
(Dated: November 6, 2018)

We present a selection of x-ray and neutron diffraction patterns of spherical (He, Ar), dumbbell- ( $N_2$ , CO), and chain-like molecules (n-C<sub>9</sub>H<sub>20</sub>, n-C<sub>19</sub>H<sub>40</sub>) solidified in nanopores of silica glass (mean pore diameter 7nm). These patterns allow us to demonstrate how key principles governing crystallization have to be adapted in order to accomplish solidification in restricted geometries. <sup>4</sup>He, Ar, and the spherical close packed phases of CO and  $N_2$  adjust to the pore geometry by introducing a sizeable amount of stacking faults. For the pore solidified, medium-length chain-like n-C<sub>19</sub>H<sub>40</sub> we observe a close packed structure without lamellar ordering, whereas for the short-chain C<sub>9</sub>H<sub>20</sub> the layering principle survives, albeit in a modified fashion compared to the bulk phase.

PACS numbers:

## I. INTRODUCTION

Simple geometric considerations along with the goal of minimizing the free energy of a system allow one to derive key principles of the microscopic architecture of crystalline, condensed matter, among them the close packing principle [1]. As the structures of simple van-der-Waals molecular crystals testify, the detailed manifestations of these building principles depend sensitively on the symmetry and the interaction of the basic building blocks (atoms, molecules or macromolecules) [2]. Here, we would like to give some flavor which key crystallization principles survive or how they have to be altered in order to allow a system to solidify in extreme spatial confinement, that is in a geometry which is restricted, at least in one direction, on the order of the size of its building blocks. Our conclusions are drawn from the study of the structure of Ar,  $N_2$ , CO, and two n-alkanes in the nanopores of silica glass. We will present the structure of the confined molecular crystals and discuss them with respect to the basic building principles established in the corresponding bulk phases. Some attention will also be paid on structural solid-solid phase transitions within the confined crystalline phases.

By filling fraction dependent measurements both on the structure [3] and on the dynamics [4] of van-der-Waals systems embedded in porous glass one can show that the pore condensates can usually be decomposed in two components: The first two or three monolayers close to the pore walls form a disordered, amorphous phase and at least for the silica matrices, no melting or freezing transitions have been observed for this component. Thus, one can term them as “dead” monolayers. By contrast, the second part of the pore filling, located closer to the pore center, leads a “life of its own” characterized by a structure and thermodynamics which are reminiscent of the bulk behavior, at least for pore diameters of the order of 10nm. In the following, we shall focus on the

structure of this second part and will refer to it as *pore solid*.

## II. EXPERIMENTAL

As hosts we have chosen either Vycor glass or a controlled pore glass (“Gelsil” from Geltech, Orlando, FL). Both substrates are practically pure fused silica. The structure of the nanopores of both matrices can be described as a network of 3D randomly oriented, connected pores with relatively uniform diameter  $d \sim 7\text{nm}$  [5]. The x-ray diffraction patterns have been recorded using a Bragg-Brentano para-focussing geometry. For more details on the experimental setup we would like to refer to ref. [3]. The elastic neutron diffraction experiment on <sup>4</sup>He has been carried out on the 2-axis diffractometer D20 of the Institut Laue Langevin, Grenoble (France). Both the neutron as well as the x-ray diffraction patterns will be presented as plots of the scattered intensity versus the modulus of the scattering vector  $q$ ,  $q = 4\pi/\lambda \sin(\Theta)$ , where  $\lambda$  corresponds to the wavelength of the x-rays and neutrons, resp. Additionally, the scattering angle  $2\Theta$  is plotted on the top axis for the x-ray diffraction patterns ( $\lambda=1.542 \text{ \AA}^{-1}$ ).

## III. RESULTS

### A. Helium and Argon

For <sup>4</sup>He the quantum mechanical zero point energy is so large compared to the normal attractive interactions that it exists as solid only under pressure  $p$  ( $p > 25\text{bar}$ ), and then with very small cohesive energies, large molar volumes and large compressibilities [2]. Bulk <sup>4</sup>He forms either a hexagonal close packed (hcp) or a body centered cubic (bcc) phase. The more loosely packed bcc-structure occurs at higher temperatures and is believed to be stabilized relative to the hcp structure for entropic reasons.

A diffraction pattern of confined <sup>4</sup>He ( $T=1\text{K}$ ,  $p=70\text{bar}$ ) is depicted in Fig 1. (a) [6]. The part of

\*E-mail: p.huber@physik.uni-saarland.de

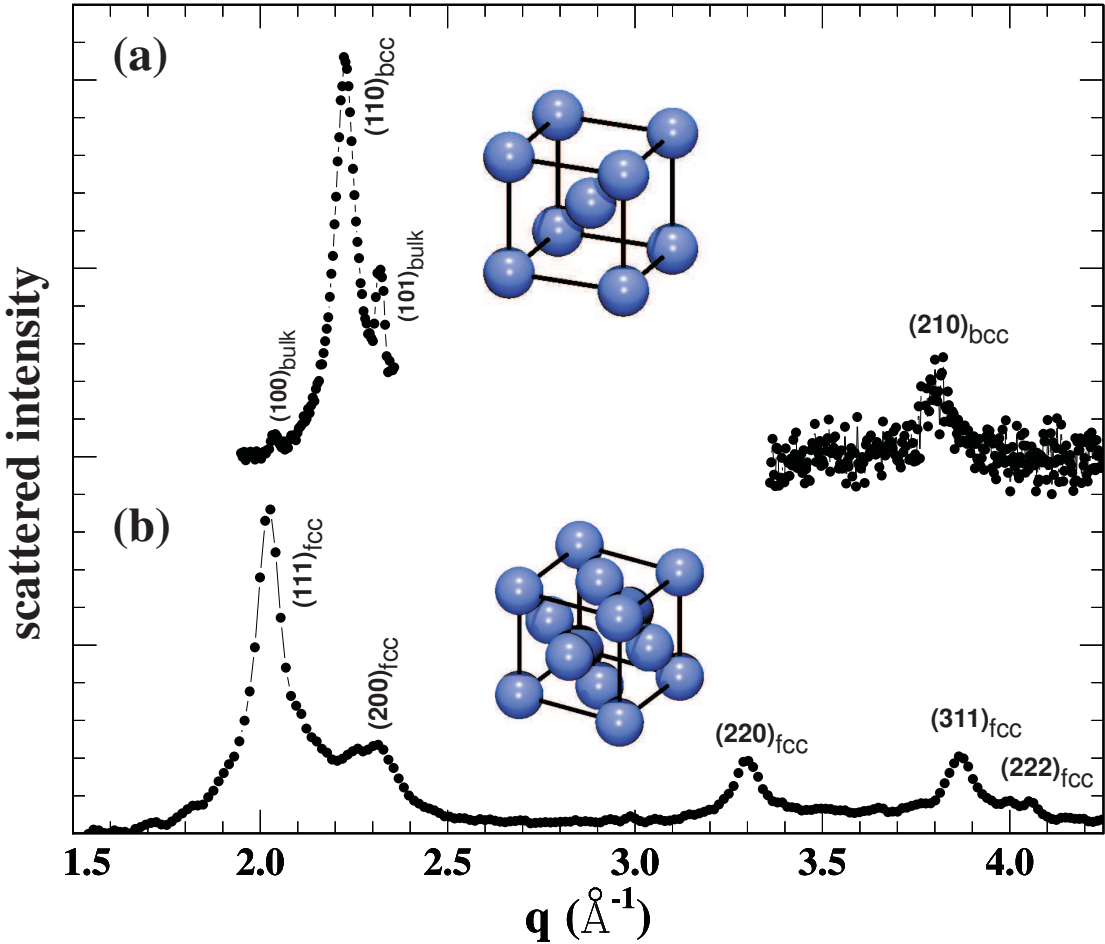


FIG. 1: (a) Neutron diffraction pattern of pore condensed  $^4\text{He}$  at  $p=70\text{bar}$ ,  $T=1\text{K}$  [6]. The reflections  $(hkl)$  are indexed on the basis of a bcc cell. The cartoon depicts the bcc structure. Note, the intensity of the  $(210)$  bcc reflection has been multiplied by a factor of 50. (b) X-ray diffraction pattern of pore condensed Ar at  $T=50\text{K}$  [3]; indicated are the fcc  $(hkl)$  reflections. As inset one can find an illustration of the fcc structure.

the pattern containing reflections from the sample cell walls and the various thermal shields ( $q$ -range from  $2.4$ - $3.5\text{\AA}^{-1}$ ) has been removed. The scattering intensity is dominated by one peak at  $q = 2.25\text{\AA}^{-1}$  that can be attributed to confined He, whereas the sharp peaks on the left and on the right wing of this peak are due to hcp bulk crystallites, sitting outside the pore space. Additionally a broad, weak peak at  $q = 3.75\text{\AA}^{-1}$  can be identified as belonging to confined  $^4\text{He}$ . A detailed analysis of the temperature dependence of the diffraction pattern that considers different packing sequences of triangular net planes (ABC stacking  $\Leftrightarrow$  fcc, AB stacking  $\Leftrightarrow$  hcp, random stacking) and the bcc structure, identifies the two observed peaks as the  $(110)$  and  $(210)$  bcc reflections. The intrinsic width  $\Delta q$  of the two peaks indicate a coherence length  $L$  of the  $^4\text{He}$  crystallites of about  $10\text{nm}$ .  $L$  is slightly larger than the pore diameter. The two Bragg peaks represent only about 30% of the pore filling, whereas the non-crystalline fraction amounts to about 70%. Additionally to two “dead” monolayers of immo-

bile molecules next to the pore walls the thermodynamic path (low  $T$ , high  $p$ ), which one has to take in order to solidify  $^4\text{He}$  in the pores leads to a liquid-like shell between the pore solid in the center of the pores and the amorphous wall coating. Further cooling below  $1\text{K}$  leads to no qualitative change of the diffraction pattern. Quite different to the situation for bulk He, the loosely packed bcc structure in the pore center is stable down to lowest temperatures. Thus, the bcc-hcp lattice reconstruction, known from bulk  $^4\text{He}$ , is suppressed in the pores.

In contrast to the quantum crystal  $^4\text{He}$  the zero point motion of the atoms of solid Ar are negligible rendering it to one of the most simple, classical crystalline solids [2]. Kept under its own vapor pressure, Ar solidifies into a fcc crystalline structure upon cooling below its bulk triple point of  $T_3^{bulk}=83.8\text{K}$ . Temperature dependent diffraction patterns of Ar confined in Vycor start to exhibit Bragg peaks upon cooling below  $76\text{K}$ , only. One observes a reduced freezing temperature in the pores. The diffraction pattern of the pore solid, as it is shown in Fig. 1(b) for  $T=60\text{K}$ , can be indexed by referring to the bulk fcc

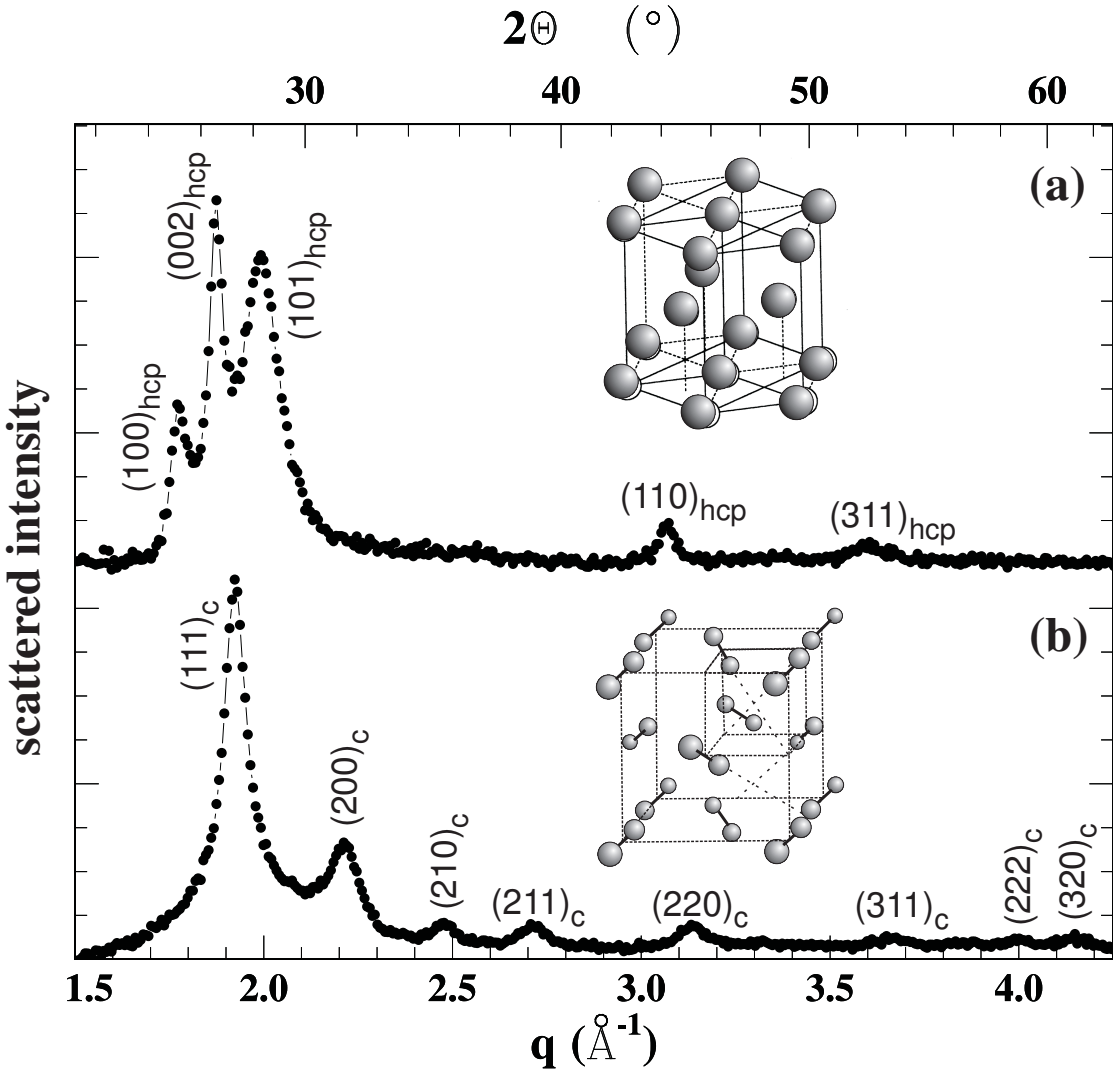


FIG. 2: (a) X-ray diffraction pattern of  $\text{N}_2$  confined in GelSil at  $T=50\text{K}$ . The reflections are indexed on the basis of a hcp lattice [7] (b) X-ray diffraction pattern of pore condensed CO at  $T=50\text{K}$ ; indicated are the Pa3 (hkl) reflections [7]. The insets in panel (a) and (b) illustrate the hcp and Pa3 structures, respectively.

Ar structure. In the accessible  $q$ -range one can identify the  $(111)$ ,  $(200)$ ,  $(220)$ ,  $(311)$  and  $(222)$  reflections. Apart from the finite size broadening, the width of the fcc reflections show a variation characteristic of crystals suffering from a substantial amount of stacking faults. If  $\alpha$  is the probability that an AB stack of triangular  $(111)$  planes is followed by a plane in the A position (hcp-like) rather than in the C position (fcc-like) and  $L$  is a characteristic crystallite size, one arrives at a satisfactory description of the diffraction pattern of the pore solid with  $L=100\text{nm}$  and  $\alpha=0.055$ . The value of  $L$  exceeds the pore diameter by far, which points again to a rather large coherence length of the crystallites along the pores.

## B. Nitrogen and Carbonmonoxide

$\text{N}_2$  and CO are molecules of similar size and shape. As bulk systems, they have closely related structural and thermodynamical properties. The melting temperatures are almost equal:  $T_3^{\text{bulk}}(\text{N}_2)=63.15\text{K}$ ,  $T_3^{\text{bulk}}(\text{CO})=68.9\text{K}$ . Bulk  $\text{N}_2$  and CO are isomorphous in both solid phases. The high-T  $\beta$ ghase is hcp with a practically ideal  $c/a$  ratio – see illustration in Fig. 2(a). Here the molecules are orientationally disordered due to rapid reorientations. At lower temperatures the bulk solids undergo a first-order phase transition into the  $\alpha$  phase (cubic, Pa3), which involves a change of the center-of-mass lattice from the hcp-stacking sequence AB... to the fcc-stacking sequence ABC... and an orientational ordering of the molecular axes, i.e. of the quadrupole moments, such that each of the four molecules of the cell points

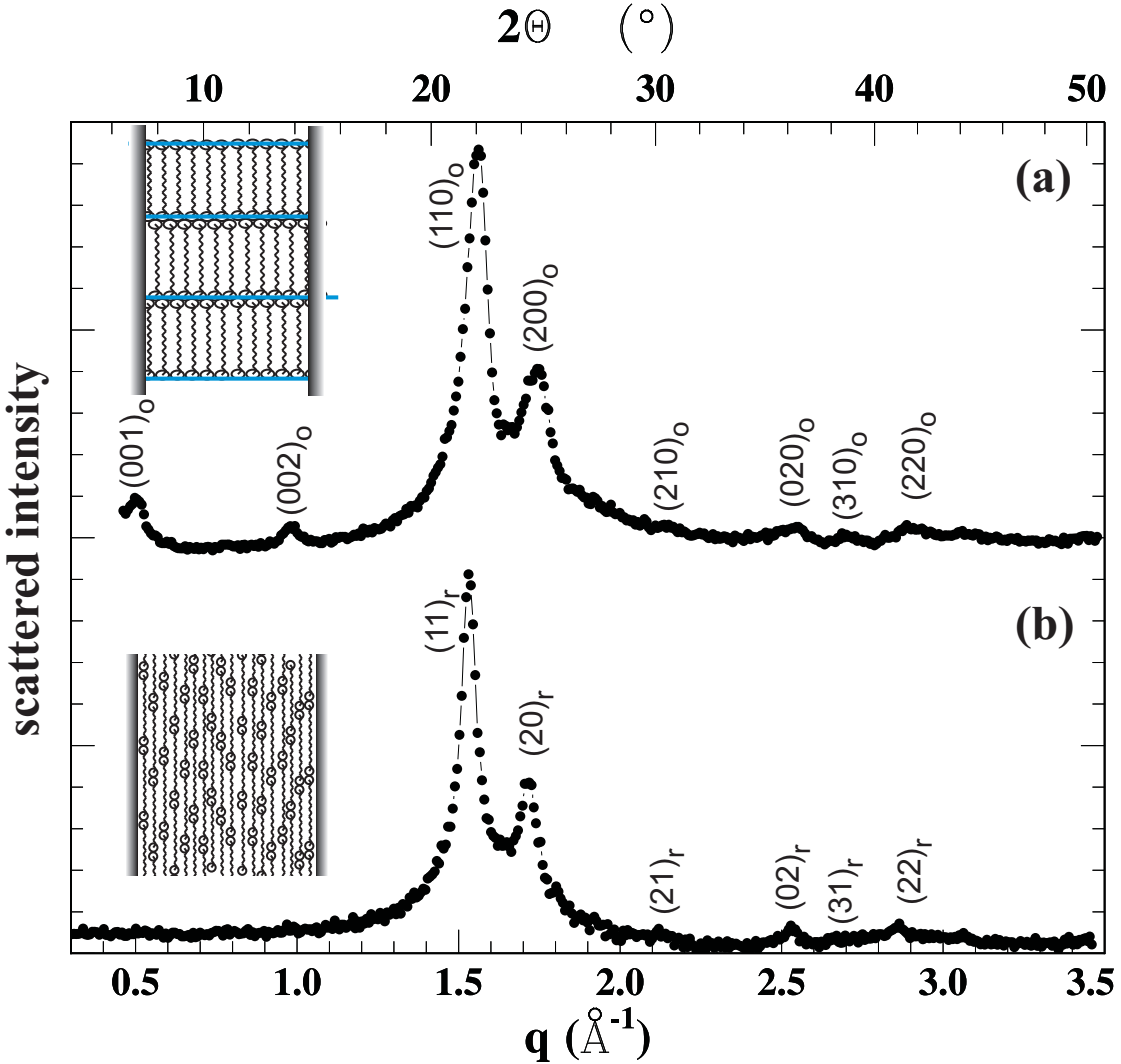


FIG. 3: (a) X-ray diffraction patterns of  $n\text{-C}_9\text{H}_{20}$  in GelSil70 at  $T=180\text{K}$ . The reflections are indexed assuming an orthorhombic unit cell. The inset depicts an illustration of the structure. The molecules' long axes are aligned parallel to the pores and obey a lamellar ordering. (b) X-ray diffraction pattern of pore condensed  $n\text{-C}_{19}\text{H}_{40}$  at  $T=200\text{K}$ . The reflections are indexed on the basis of a two-dimensional rectangular mesh. The cartoon depicts the "nematicocrystalline" state of the pore solid [9].

along one of the four  $\langle 111 \rangle$  directions – compare illustration in Fig. 2(b). This orientation of the molecules appears as a compromise of the cubic symmetry of the center of mass lattice and the quadrupolar part of the interaction of the molecules: The resulting mutual orientation of the long axes of the molecules is given by the tetrahedral angle of 109 degrees, which is reasonably close to an angle of 90 degrees minimizing their quadrupolar interaction. Solidification of  $\text{N}_2$  in GelSil, indicated by the appearance of the hcp Bragg peaks, occurs at  $T=54\text{K}$ . The diffraction pattern of confined  $\text{N}_2$  shows five Bragg peaks, which all coincide with reflections of bulk hcp  $\beta\text{-N}_2$ , although with altered intensity ratios and enhanced linewidths compared to the pattern of the bulk phase. The  $(102)$  reflection is missing. The  $(103)$  reflection is extremely broadened, but can be still identified. By contrast, the  $(002)$  reflection dominates

the diffraction pattern and is remarkably sharp. The variation of the intrinsic peak width  $\Delta q$  as a function of the crystallographic direction can be described by a preferred growth of the crystallites with their c-axes along the pores and a sizeable amount of stacking faults in the pore solid. This conclusion is corroborated by diffraction studies varying the pore diameter as well as studies of  $\text{N}_2$  in well-aligned pores of porous silicon [8]. Thus, pore confined nitrogen establishes a structure very related to the bulk  $\beta$  phase. Upon cooling, however, no transition into the orientational ordered  $\alpha$  phase has been observed. This solid-solid transition could be investigated for pore confined CO, only. It forms the same hcp phase as just presented for confined  $\text{N}_2$ , however, at  $T=54\text{K}$  the center of mass lattice rearranges according to the  $\beta\text{-}\alpha$  phase transition scenario and for  $T<54\text{K}$  one observes a diffraction pattern typical of the cubic  $\text{Pa}3$  structure – compare

Fig. 2(b). As a peculiarity of confined CO the occurrence of a fcc phase upon heating has been found. The orientational order of the molecules is lost while maintaining the cubic lattice.

### C. Nonane and Nonadecane

In the following we focus on the structure of more complex molecular crystals, built out of chain-like molecules, where the length  $l$  of the rectified molecules is of the order of the pore diameter. We have chosen the linear hydrocarbons  $n\text{-C}_9\text{H}_{20}$  and  $n\text{-C}_{19}\text{H}_{40}$  with  $l=1.3\text{ nm}$  and  $l=2.6\text{ nm}$ , resp. The C atoms of the zigzag backbone of these linear hydrocarbons are all in the trans-configuration, so all of them are located in a plane. The molecular crystals form layered structures. For  $n\text{-C}_{19}\text{H}_{40}$  the molecules are aligned perpendicular to the layers. Within the layers the molecules are close packed, side by side, in a quasi-two-dimensional array. For low temperatures the azimuth of the rotation of the  $-\text{C-C-}$  plane around the long  $z$ -axis of the molecules alternates in a herringbone fashion. In the short-length  $n\text{-C}_9\text{H}_{20}$  the molecules are tilted by about  $15\text{ deg}$  with respect to the layer normals.

The diffraction pattern of confined  $n\text{-C}_9\text{H}_{20}$  – see Fig. 3 – indicates a layering of the molecules (two peaks at low  $q$ ) and additionally a herringbone type ordering of the molecules within the layers (6 peaks at  $q>1.4\text{ \AA}^{-1}$ ). The reflections at higher  $q$  can be indexed as  $(hk0)$  in terms of an orthorhombic unit cell. This means that any correlations of the lateral positions of the layers are lost in the pores. If such correlations existed, peaks of the type  $(hkl)$ ,  $l<>0$  should show up. Moreover, the layering distance extracted from the  $(001)_o$  and  $(002)_o$  peaks at low  $q$  agree with the length of the rectified molecules, thus the confinement imposes an alignment of  $n\text{-C}_9\text{H}_{20}$  parallel to the layer normal. Presumably, the layer normals are oriented parallel to the pore axis, which results in a structure reminiscent of the crystal-E phase of rod-like liquid crystals [10].

As can be seen by a comparison of Fig. 3(a) and (b) the diffraction pattern of  $n\text{-C}_{19}\text{H}_{40}$  is identical to the one of  $n\text{-C}_9\text{H}_{20}$  except for the missing  $(001)$  layering peaks at low  $q$  ( $q<1.4\text{ \AA}^{-1}$ ). The resulting structure of confined  $n\text{-C}_{19}\text{H}_{40}$  is depicted in Fig. 3(b): The molecules' position along the pore axes have no correlations. One basic ordering principle of the bulk crystalline alkane, i.e. the layering, is suppressed, rendering the system effectively two-dimensional (2D) [9]. Moreover, an analysis of the coherence length of the 2D crystals based on the width of the  $(hk)_r$  reflections yields  $7.5\text{ nm}$ . This value is close to the mean pore diameter, which suggests an alignment of the molecules along the pore axis. Isomorphous structures, termed “nematocrystalline”, have been reported for the bulk phases of natural waxes, e.g. bee wax, consisting of complicated mixtures of chain-like molecules, among them alkanes [11].

### IV. SUMMARY

Spherical close-packed structures can accommodate to the pore geometry by introducing of a sizeable amount of stacking faults. The structures of the confined chain-like molecules is affected in a more drastic way, in particular the anisotropic pore structure calls for an alignment of the molecules parallel to the pore axes. Nevertheless, the structures follow the close packing principles; even the medium-length  $n\text{-C}_{19}\text{H}_{40}$  pursues this concept by establishing a “nematocrystalline” state.

Extreme cases of structural disorder such as random-stacking or random close packing have not been found for the pore solids investigated. The preference to form structures with higher symmetry obeying subtleties of the symmetry of the molecules' interaction potentials, which lead to the fcc-Ar, hcp- or bcc-  $\text{N}_2$ , CO, and  $^4\text{He}$ , resp. and finally to the herringbone-type ordering of the linear hydrocarbon chains, prevails even for the crystallization in nano-confinement. If one considers the distribution of the pore diameters and the tortuosity of the pores, in general all deviations of the employed porous hosts from an idealized pore space which presumably additionally favor disordered structures, our findings testify even more to the robustness of the basic crystallization principles. As witnessed by the suppression of the bcc-hcp transition in confined He, the absence of the  $\alpha\beta$  transition in confined  $\text{N}_2$ , and the occurrence of a fcc-CO phase in the pores, the phase sequence in the pores can nevertheless be significantly affected by the confinement. For pore condensates embedded in well-defined nanopores of template grown MCM-41 or SBA-15 silica matrices [12] quite similar structures have been observed [13]. Thus, the detailed geometry and topology of the matrix is of minor importance for the crystallization; they are, however, crucial for an understanding of the thermodynamical aspects of pore condensates, e.g. the freezing/melting process or condensation/sublimation phenomena in the pores [14].

Another interesting aspect concerns the thermodynamic stability of pore condensates. There is agreement that capillary condensed cryogenic liquids such as Ar, He, CO and  $\text{N}_2$  are stable in mesoporous glasses such as Vycor. In the solid regime, however, several authors report changes that have been interpreted by a migration of the filling out of the pores and have been referred to as “mobility transition”, a “new type of structural phase transition”, and “dewetting transition” [15]. We could not find any hints for such transitions of the cryosolids investigated. Nevertheless, we would like to mention that we gather increasing evidence for a thermodynamic metastability of the solid phases of medium- and long-chain n-alkanes in an ongoing study aimed at an understanding of the structure and thermodynamics of hydrocarbons in nanopores.

Finally we would like to mention that studies on crystallization or, more generally spoken, structural transitions in nanoconfinement are not only interesting by

their own virtue, but also of relevance for such different phenomena as friction, frost heave, transport through biomembranes, and crystal growth [16]. For instance, recently the immobilization and crystallization of proteins in nanopores of Vycor and porous silicon attracted attention in the flourishing field of structural genomics [17]. It could be demonstrated that these pore confined protein structures promote the formation of protein bulk crystal-

lites, one of the pivotal goals in this area of science.

### Acknowledgments

This work has been supported by the Deutsche Forschungsgemeinschaft (SFB 277).

---

[1] M. J. Buerger, *Elementary crystallography*, J. Wiley and Sons, NY (1963).

[2] *Rare Gas Solids*, M. L. Klein, J. A. Venables eds., Academic Press, London (1977); N. G. Parsonage and L.A. K. Staveley, *Disorder in Crystals*, Clarendon, Oxford (1978).

[3] P. Huber and K. Knorr, Phys. Rev. B **60**, 12657 (1999).

[4] J. Baumert, B. Asmussen, C. Gutt, and R. Kahn, J. Chem. Phys. **116**, 10869 (2002).

[5] P. Levitz, G. Ehret, S. K. Sinha, and J. M. Drake, J. Chem. Phys. **95**, 8 (1991).

[6] D. Wallacher, M. Rheinstaedter, T. Hansen, and K. Knorr, J. Low Temp. Phys., **138**, 1013 (2005).

[7] P. Huber, D. Wallacher, and K. Knorr, Phys. Rev. B **60**, 12666 (1999).

[8] T. Hofmann, D. Wallacher, P. Huber, and K. Knorr, J. Low Temp. Phys., **140**, 91 (2005).

[9] P. Huber, D. Wallacher, J. Albers, and K. Knorr, Europhys. Lett. **65**, 351 (2004).

[10] S. Kumar, "Liquid Crystals", Cambridge University Press, Cambridge (2001).

[11] D.L. Dorset, J. Phys. D **32**, 1276 (1999).

[12] D.Y. Zhao, J.L. Feng, Q.S. Huo, N. Melosh, G.H. Fredrickson, B.F. Chmelka, G.D. Stucky, Science **279**, 548 (1998); C. T. Kresge, C.T. et al. Nature **359**, 710 (1992).

[13] K. Morishige and K. Kawano, J. Phys. Chem. B **104**, 2894 (2000). K. Morishige and Y. Ogiu, J. Chem. Phys. **114**, 7166 (2001); K. Morishige and H. Uematsu, J. Chem. Phys. **122**, 044711 (2005).

[14] H. K. Christenson, J. Phys. Cond. Matt. **13**, R95 (2001); D. Wallacher and K. Knorr, Phys. Rev. B **63**, 104202 (2001); V. Sopranyuk, D. Wallacher, P. Huber, K. Knorr, and A.V. Kityk, Phys. Rev. B **67**, 144105 (2003); D. Wallacher, N. Kunzner, D. Kovalev, N. Knorr, and K. Knorr, Phys. Rev. Lett. **92**, 195704 (2004).

[15] D.E. Silva, P.E. Sokol, S.N. Ehrlich, Phys. Rev. Lett. **88**, 155701 (2002), D. W. Brown, P.E. Sokol, S. N. Ehrlich, Phys. Rev. Lett. **81**, 1019 (1998); M. Schindler et. al., Phys. Rev. B **53**, 11451 (1996).

[16] M. Urbakh, J. Klafter, D. Gourdon, and J. Israelachvili, Nature **430**, 525 (2004); K. Murata et al. Nature **407**, 599 (2000); N. E. Chayen, Current Opinions in Structural Biology **14**, 577 (2004).

[17] N.E. Chayen, E. Saridakis, R. El-Bahar, and Y. Nemirosky, J. Mol. Biology, **312**, 591 (2001); L. Rong, H. Komatsu, I. Yoshizaki, A. Kadokawa, and S. Yoda, J. Synchr. Radiation News **11**, 27 (2004).